



Multiple high-temperature transitions driven by dynamical structures in NaI

M. E. Manley,^{1,*} J. R. Jeffries,² H. Lee,³ N. P. Butch,^{4,5} A. Zabalegui,³ and D. L. Abernathy¹

¹*Oak Ridge National Laboratory, Oak Ridge, Tennessee 37831, USA*

²*Lawrence Livermore National Laboratory, Livermore, California 94550, USA*

³*Santa Clara University, Santa Clara, California 95053, USA*

⁴*Department of Physics, Center for Nanophysics and Advanced Materials, University of Maryland, College Park, Maryland 20742, USA*

⁵*NIST Center for Neutron Research, National Institute of Standards and Technology, Gaithersburg, Maryland 20899, USA*

(Received 25 May 2014; published 27 June 2014)

Multiple, consecutive high-temperature transitions in NaI involving dynamical order and/or localization in the energy-momentum spectrum but not in the average crystal structure are revealed by lattice dynamics, x-ray lattice spacing, and heat-capacity measurements. Distinctive energy-momentum patterns and lattice distortions indicate dynamical structures forming within randomly stacked planes, rather than the isolated point-defect-like intrinsic localized modes predicted. Transition entropies are accounted for by vibrational entropy changes, and the transition enthalpies are explained by the strain energy of forming stacking-fault-like planar distortions deduced from x-ray-diffraction peak shifts. The vibrational entropy of the dynamical structures stabilizes surrounding elastic distortions.

DOI: [10.1103/PhysRevB.89.224106](https://doi.org/10.1103/PhysRevB.89.224106)

PACS number(s): 63.20.Pw, 63.20.dd, 63.20.Ry, 78.70.Nx

I. INTRODUCTION

Solid-state phase transitions are typically characterized by changes in crystal, electronic, or magnetic symmetries [1], whereas the lattice-dynamical symmetry is assumed to follow the parent structures [2]. Whereas for harmonic vibrations this *must* be true, it need not be for anharmonic lattices [3]. Intrinsic localized modes (ILMs)—also known as discrete breathers [3]—are spatially localized anharmonic vibrations that break translational symmetry. Until recently, however, equilibrium ILMs were thought to occur as random pointlike features stabilized by configurational entropy [4], but neutron-scattering experiments indicate that ILMs in NaI [5] may form in a long-range dynamical pattern [6]. This periodic break in translational symmetry is only observable in the energy-momentum spectrum, not in the average crystal structure [6]. This condition of dynamical order is reminiscent of the recently proposed idea of time [7,8] or space-time [9] crystals, except those proposals were for orbits of broken symmetry in the ground state or pseudoground state [9], not in thermal equilibrium. For a ground-state space-time crystal to exist, the theoretical challenge is finding a system where the lowest-energy state exhibits space-time ordering, such as a ground state that includes a soliton traveling around a ring [7]. In the case of equilibrium dynamical structures, the challenge lies in understanding how vibrational energy can form an organized pattern distinct from the crystal structure while also maintaining the thermodynamically required condition of energy equipartition [6].

Although it is clear that stable ILM solutions exist for crystals, in that they can be generated in realistic driven models [3], how they form in thermal equilibrium remains a topic of debate. Using molecular dynamics simulations of diatomic crystals Khadeeva and Dmitriev [10] found that ILMs increase exponentially in both concentration and lifetime with increasing temperature and Kistanov and Dmitriev [11] found

that ILMs form spontaneously in crystals with the NaI structure at about the same temperature observed experimentally [5]. On the other hand, in a recent paper Sievers *et al.* [12] estimate the kinetic energy of an ILM in NaI and argue that the value is too large for a significant concentration of ILMs to be thermally stabilized by configurational entropy below the melting temperature (kinetic energy is constrained by temperature, see Ref. [13]). However, for NaI the observation of coherent dynamical structure at high temperatures [6], which implies order, shows that these observed dynamical features are not stabilized by configurational-disorder entropy. Indeed, here we show that entropy changes associated with these dynamical structures are explained by vibrational entropy alone and that the internal energy changes are explained by the energy of stacking-fault-like distortions that form concomitant with planar-shaped dynamical structures. The energetics of these planar dynamical structures are also expected to be quite different from that of isolated pointlike ILMs modeled up to this point. At higher temperatures, the planar dynamical structures exhibit phase transitions with the requisite peaks in the heat capacity. Heat-capacity, x-ray lattice spacing, and additional neutron-scattering measurements indicate that similar transitions with dynamical structures occur repeatedly with increasing temperatures once they begin.

Recently, Kempa *et al.* [14] reported independent neutron-scattering measurements showing the absence of the 10.3-meV gap ILM at 600 K near $Q = [2.5, 2.5, 1.5]$, the Q point where it was observed at 575 K in Ref. [5]. On the other hand, they do observe the 10-meV gap ILM* feature [6] at 636 K at both $Q = [2, 2, 1]$ and $Q = [3, 3, 2]$, similar to that observed at these Q points measured at 636 K in Ref. [6] (Note: Temperature accuracy at these temperatures is typically only good to within ± 10 K). Interestingly, abrupt disappearance and reappearance of the original gap ILM with similarly small temperature differences were also documented in Ref. [6]; when viewed along [111] the ILM feature appears at 614 K, disappears at 636 K, then fully reappears at 659 K, and the behavior is reversible on cooling [6]. The

*Corresponding author: manley@ornl.gov

disappearance of the ILM peak along [111] at 636 K coincides with the appearance of ILM* along [110] at $Q = [2,2,1]$ and $Q = [3,3,2]$ and was interpreted as a collective reorienting of the dynamical structure [6]. In this context, it is not surprising that the ILM feature appears at 575 K [5] but not at 600 K at $Q = [2.5,2.5,1.5]$ [14] since a similar reorientation is possible. The fact that the ILM* feature is observed at 636 K in Ref. [14] is consistent with this interpretation. However, the analysis of the results in Ref. [14] did not include a correction for incoherent scattering as was performed in Refs. [5,15], making their interpretation somewhat inconclusive [14]. As first pointed out in Ref. [15], because the incoherent scattering has a Q -independent structure it can be isolated by measuring parts of reciprocal space that do not include scattering from coherent phonons, such as near zone centers [15]. However, the incoherent scattering from NaI (mostly from Na) is related to the neutron-cross-sectional-weighted phonon density of states [15], which has a minimum at the spectral gap centered around 10 meV, not a peak [5], so the incoherent scattering from NaI could not be responsible for a gap peak. Scattering from small amounts of hydrogen was also suggested as a possible artifact [14], but 10 meV is too low to be from H vibrations, and because H scatters incoherently any contribution it makes would also have been removed using the incoherent correction procedure discussed above. Hence, considering all the data in Refs. [5,6,14], gap peaks near ~ 10 meV appear in data from four different instruments at four different neutron facilities on multiple crystals and a powder but with an unexpectedly complex temperature dependence where the dynamical structure changes every 20 K or so. This temperature dependence is so unusual, and perhaps even hard to believe, that it warrants further investigation. This paper shows that the complex temperature dependence is a manifestation of a series of consecutive transitions driven by the vibrational entropy of forming various partially ordered lattice-dynamical structures at high temperatures.

II. EXPERIMENT

Neutron-scattering spectra were obtained on large single crystals of NaI(0.002Tl) (the same source as in Ref. [5]) and pure NaI mounted in a rotating furnace using the wide Angular-Range Chopper Spectrometer at the Spallation Neutron Source of Oak Ridge National Laboratory. Empty can measurements were collected at each temperature and were subtracted from all data sets. Measurements were taken with (H, K, and L are Miller indices) in the scattering plane, and Q - E volumes of data were obtained at 567, 636, and 659 K by rotating the angle between [100] and the incident beam in 1° steps, collecting a scan at each angle, and stitching the data together using the MSlice software package in DAVE [16]. The angles ranged from 70° to 100° for 567 K and between 65° and 105° for 636 and 659 K.

Angle-dispersive x-ray-diffraction data were acquired in a transmission geometry using a microfocused ($50 \times 50 \mu\text{m}^2$) x-ray beam with an incident wavelength of 0.4133 \AA (30 keV) on the High-Pressure Collaborative Access Team (HPCAT) beamline (Sector 16) at the Advanced Photon Source. Diffraction patterns were collected on a MAR345 image plate using 20–30-s exposure times. The NaI(0.002Tl)

single crystal was loaded into a small water-cooled vacuum chamber equipped with an internal cartridge heater and type- K thermocouple. The vacuum chamber was constructed with Kapton-film windows for the incident and diffracted beams. The temperature was controlled to within 100 mK using a Lakeshore LS-340 temperature controller. The two-dimensional (2D) diffraction patterns were integrated with the program FIT2D to yield conventional one-dimensional intensity versus 2Θ patterns.

The laser flash technique, which was originally developed to characterize thermal diffusivity of a plate sample, was also used here to determine the heat capacity. As one side is heated by an instantaneous heat source, the temperature on the other side will rise at a rate determined by the sample's diffusivity and heat capacity. By measuring transient response and the maximum temperature value at the backside, thermal diffusivity and heat capacity can be evaluated, respectively. The Cape-Lehman model with pulse correction [17] was used to analyze these properties using a Netzsch *LFA 457 Microflash*. For heat capacity, Pyroceram 9606 was used as a reference sample. Samples were cut into 10-mm squares about 1-mm thick, sanded until their surfaces were parallel, and coated with 123[®] graphite spray to ensure the same surface conditions between our sample and the reference sample. To ensure surfaces were opaque additional samples were prepared with coatings of platinum metal followed by the same graphite coating. To rule out effects of heat lost to surface damage, measurements were also repeated with the heating pulse reduced in power by a factor of 4 (this is the difference between lowest and highest settings in the Netzsch *LFA 457 Microflash*). Additional heat-capacity measurements were performed with a PerkinElmer differential scanning calorimeter (DSC) with a heating rate of 10 K/min. A limitation of the DSC realized here is that in cases where there are multiple consecutive phase transitions as a function of temperature intrinsic "temperature smearing" [18] tends to washout details, which is the reason the laser flash technique is used in conjunction with DSC measurements.

III. RESULTS

A. Calorimetry

The laser flash calorimetry measurement results shown in Fig. 1(a) appear as an up-sloping smooth curve with a gradually decreasing slope from about 550 K up to about 610 K where the curve then turns up sharply into a peak centered near 620 K, followed by additional consecutive peaks at ~ 645 , ~ 660 K, and probably the beginnings of a fourth peak around 690 K. These sharp peaks were reproduced on three different crystals, each of which had either a different coating or a laser flash pulse power, and all three were measured three times each (for a total of nine separate measurements at each temperature). Each point shown is an average of the three measurements on the same crystal, and the error bars are the standard deviations. The integrated area under each peak corresponds to only about $0.02 k_B/\text{atom}$, which is much smaller than the entropy change associated with a typical configurational disorder-driven transition (e.g., two configurations per atom correspond to $\sim 0.69 k_B/\text{atom}$). These peaks correspond to abrupt changes in the dynamical structure, illustrated in Fig. 1(c) and discussed in more detail below. The

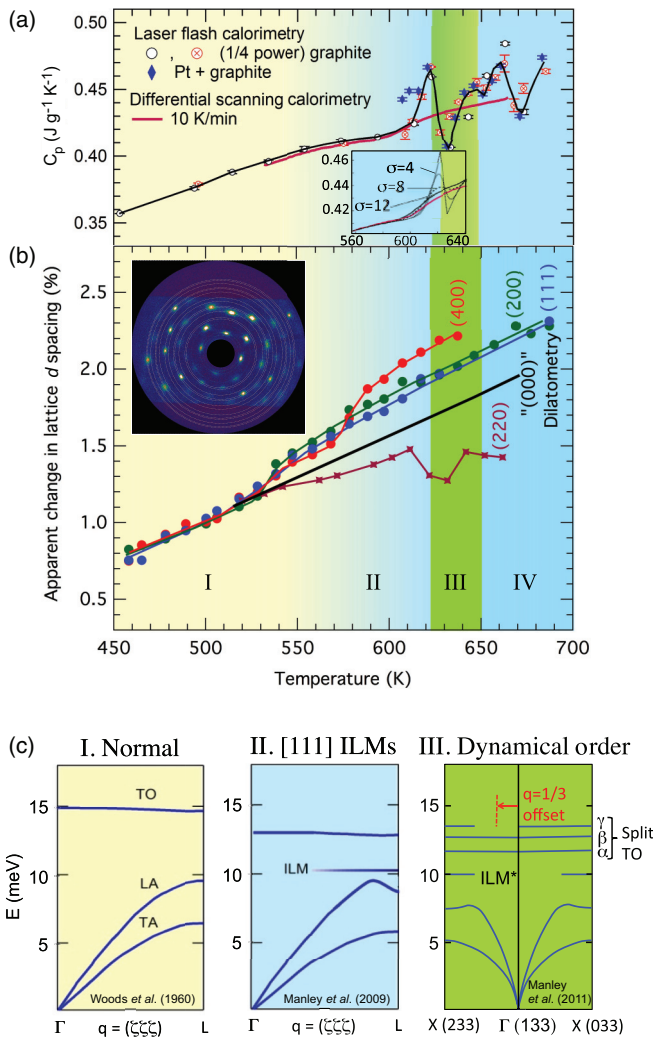


FIG. 1. (Color online) A summary of the measurements performed on crystals of pure NaI [results were not noticeably different with NaI(0.002Ti)]. (a) Heat capacity measured using both a laser flash (symbols) and the DSC (solid dark red line). The solid black line is a guide to the eye for the laser flash calorimetry data points. The inset shows how convoluting the laser flash data with Gaussian temperature smearing functions—with widths $\sigma = 4, 8,$ and 12 K—produces improved agreement with the DSC measurement; $\sigma \sim 12$ K is in very good agreement with the DSC data. (b) Percent change in the lattice d spacing determined from the positions of several single-crystal diffraction peaks indicated as well as from the dilatometry measurements (the dilatometry is labeled “(000)” because the macroscopic measurement scale corresponds to effectively infinite d spacing or zero in reciprocal units). The inset shows a two-dimensional x-ray-diffraction pattern from single-crystal NaI at ambient temperature; the orientation of the crystal is close to the [100] direction. The dashed light-orange rings represent the Bragg reflections for the NaI crystal structure. The three innermost rings, corresponding to the (111), (200), and (220) reflections, are excluded to show faint powder rings that arise from the sample surface. (c) Schematic summary of the lattice-dynamical structures reported in different temperature ranges; Region “I. Normal” is based on the measurements of Woods *et al.* [15] and Manley *et al.* [5]; Region “II. [111] ILMs” is based on the measurements of Manley *et al.* [5]; and Region “III. Dynamical order” is based on the measurements of Manley *et al.* [6].

measured DSC curve also shown in Fig. 1(a) matches the broad shape of the laser flash calorimetry but does not show the consecutive sharp peaks. Assuming a Gaussian temperature broadening function for the DSC [18], however, the laser flash calorimetry results smooth out and come into close agreement with the DSC for a smearing width of 12 K, see the inset. Hence, with smearing, the signature of the changes in the DSC is just a smooth step up in the heat-capacity curve with the onset of the consecutive peaks observed in the laser flash heat capacity.

B. X-ray diffraction

The single-crystal diffraction patterns from the NaI crystals (performed both with and without 0.002Ti) [Fig. 1(b) inset] show no obvious changes in symmetry on heating. The overall pattern can be fit with the usual NaCl salt structure at all temperatures measured from 300 to 690 K. However, the temperature dependence of individual reflections that could be accurately determined at most temperatures, including (200), (111), (220), and (400), show distinct anomalies in their apparent d -spacing temperature dependencies [Fig. 1(b)], and these coincide with anomalies in the dynamical structure [illustrated in Fig. 1(c)] and the heat capacity [Fig. 1(a)]. Figure 1(b) shows the temperature dependence of the percent change in the apparent d spacing, which is determined from the position of the sharp reflection center (following the procedure described by Warren [19] for characterizing distortions associated with stacking faults). Below ~ 540 K all of the reflections produce values that fall onto a single line, a line that is in good agreement with the behavior expected from bulk dilatometry measurements. Just above 540 K, however, the (111), (200), and (400) apparent d spacings gradually overexpand about 0.2% whereas the (220) overcontracts by about 0.15%. This temperature range is where the ILM feature first appears along the [111] direction at 575 K [5] as illustrated in Fig. 1(c) (region II). These relative shifts in different order Bragg reflections are similar to what is expected with the phase-shifting effect associated with stacking faults [19]. Around ~ 590 K the (400) apparent spacing further overexpands again. This expansion occurs between the temperature where the ILM is observed at ~ 575 K in Ref. [5] and where it is not observed at ~ 600 K in Ref. [14] at the same point $Q = [2.5, 2.5, 1.5]$. Between 610 and 620 K the (220) apparent d spacing overcontracts abruptly by $\sim 0.3\%$. This abrupt contraction coincides with the first sharp peak in the heat capacity [Fig. 1(a)] and the transition from the single ILM feature (region II) to the more complex dynamically ordered state (region III), which was interpreted as a dynamical superlattice of ILMs in Ref. [6]. Between 630 and 645 K the (220) apparent d spacing abruptly expands by about 0.3%, effectively undoing much of the contraction that occurs between 610 and 620 K. This abrupt expansion coincides with the second peak in the heat capacity [Fig. 1(a)] and the transition from the complex dynamically ordered state (region III) back to a single ILM feature (region IV) [6] [also in Fig. 2(a)]. This observation suggests that the temperature range of the dynamically ordered state is only about 10 K, which is even narrower than the lattice dynamics indicated in going from region II at 614 K to region III at 636 K and

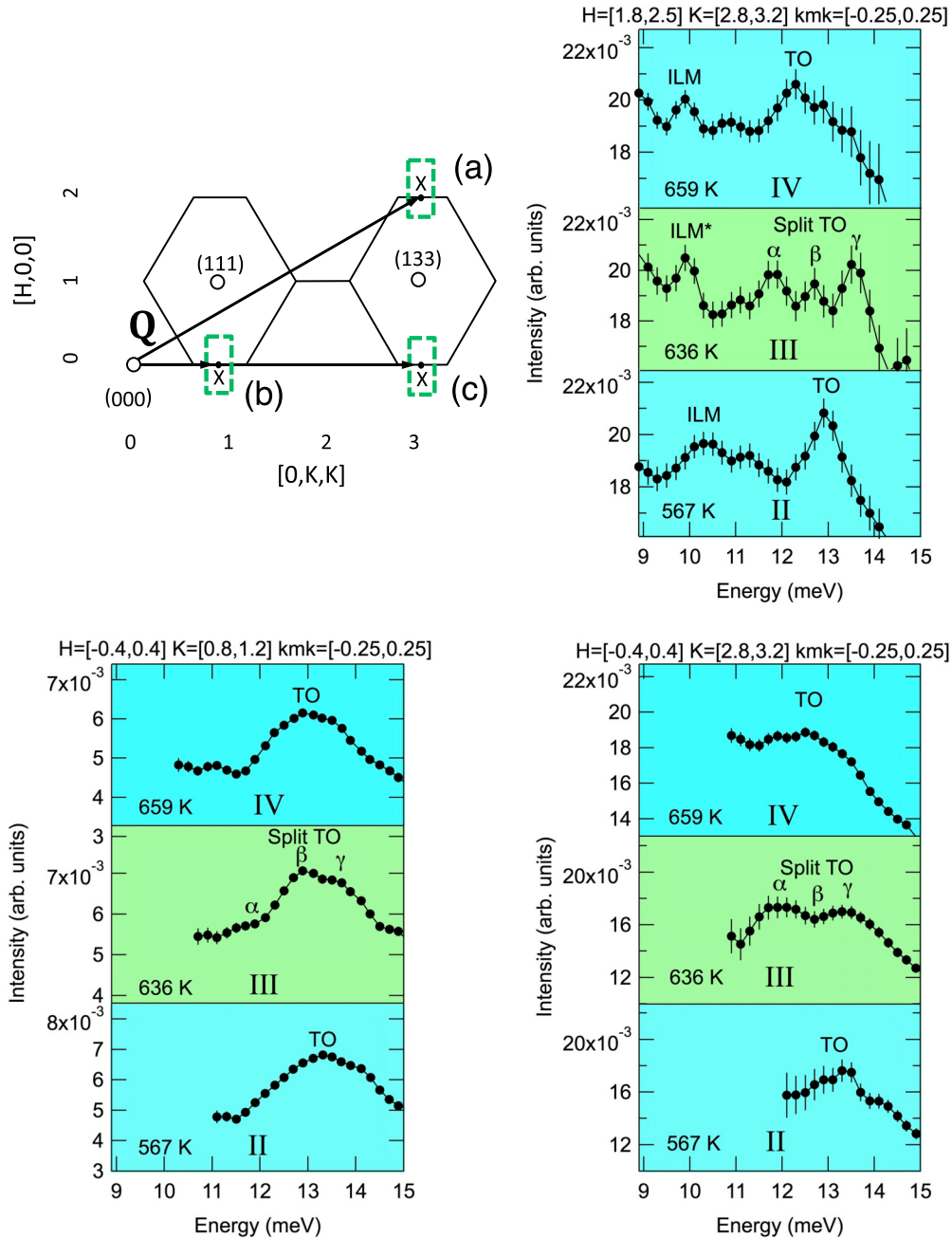


FIG. 2. (Color online) Inelastic-neutron-scattering measurements on NaI(0.002Ti) crystals collected around three high symmetry X points: (a) (233), (b) (011), and (c) (033). The “cuts” from the time-of-flight neutron-scattering data are integrated over the dashed green boxes shown in the illustration and are indicated numerically in the header of each panel. The out-of-plane direction, labeled kmk for $[0, K, -K]$, is integrated over ± 0.25 reciprocal lattice units.

then to region IV at 659 K in Ref. [6]. It was speculated that narrowness of the ordering region was due to a rational concentration fraction of ILMs being reached, in analogy with ordering at $1/3$ or $1/2$ atomic species fractions in binary alloys [6]. Given this narrow ordering temperature range, the expected ± 10 -K uncertainty in the temperature measurement for neutron-scattering experiments is large enough to explain why the fragmentation of the transverse optic (TO) mode reported at 636 K in Ref. [6] was missing in Ref. [14]. Clearly, tight temperature control is needed to accurately characterize this complex behavior in the dynamical structure.

C. Inelastic neutron scattering

Figure 2 shows the temperature dependence of the lattice-dynamical structure near three high symmetry X points, (233), (011), and (033). The behavior at 567 K (region II) and 636 K (region III) was mapped out in full detail in Ref. [6] as summarized in Fig. 1(c), but the behavior at these same X points at 659 K (region IV) is a new detail. In Ref. [6] it was shown that the single ILM feature recovered at 659 K but only in narrow off-symmetry regions of energy-momentum space explored using just one crystal orientation. The new data show that the dynamical structure at 659 K essentially recovers the

same basic structure observed at 567 K at multiple equivalent Q points; a single TO and a single gap mode (ILM) can be observed. The fragmentation of the TO mode, a characteristic of ordering [6], is no longer evident. The energy positions of all the features do, however, shift somewhat with temperature. At 567 K the ILM peak is at 10.3 ± 0.1 meV, and the TO mode is at 13 ± 0.1 meV. At 636 K the ILM* peak is at 10 ± 0.1 meV, and the TO is split into three peaks at 11.8 ± 0.1 , 12.8 ± 0.1 , and 13.5 ± 0.1 meV (there is also a lower-symmetry coherent structure associated with these features [6]). Finally, at 659 K the ILM is at 9.9 ± 0.1 meV, and the recovered single TO is at 12.3 ± 0.1 meV.

IV. ANALYSIS

A. Transition entropy from lattice vibrations

To explain the entropy changes associated with the small peaks in the heat capacity [Fig. 1(a)], we estimate the vibrational entropy changes from the corresponding changes observed in the vibrational spectrum (Fig. 2). The entropies of the transitions are challenging to quantify from both the perspective of the overlapping peaks on an irregular background in the heat capacity [Fig. 1(a)] and the vibrational entropies estimated from changes in the vibrational spectrum (Fig. 2). Nevertheless, carving out an area under each peak can provide an estimate of the total entropy change across each peak as depicted in Fig. 3. Furthermore, the vibrational entropy changes can be estimated by assuming that only the changes in the ILM, TO phonon, and associated TO phonon fragments (α, β, γ) are important (Fig. 3). This assumption is supported by the fact that no changes were observed in the transverse acoustic (TA) or longitudinal acoustic (LA) modes across these temperatures in Ref. [6].

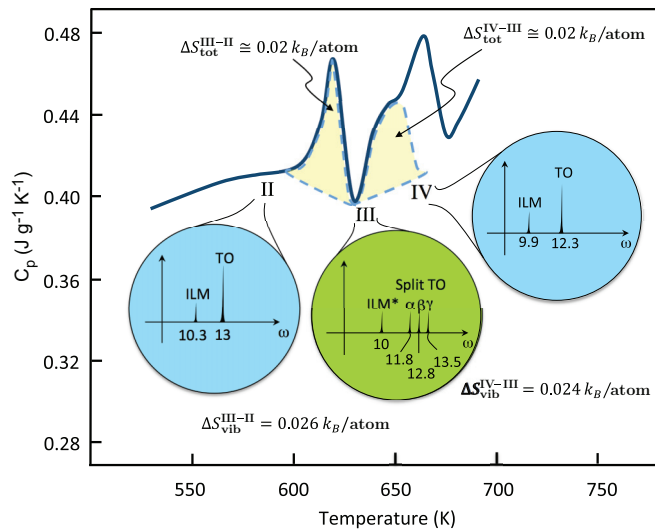


FIG. 3. (Color online) Comparison of the total transition entropies estimated from the features in the laser flash calorimetry data [Fig. 1(a)] with the vibrational entropy changes estimated from the vibrational spectral features associated with the formation and breakup of the dynamical superlattice structures from Fig. 2. The values are consistent. See text for calculation details.

The total transition entropy ΔS is estimated by integrating the areas highlighted in Fig. 3 using the standard expression for entropy in terms of heat capacity,

$$\Delta S = \int \frac{C_p}{T} dT. \quad (1)$$

The resulting entropy values for the first two transition peaks are both $0.02 \pm 0.005 k_B/\text{atom}$. The uncertainty in these numbers is based on the uncertainty in the baseline, not from the statistical noise in the data, which is a smaller effect.

To estimate the vibrational entropy changes from changes in the ILM, TO phonon, and TO fragments we first assume that the parts are all derived from the parent TO phonon so that states of the parent TO phonon are transferred to the ILM and TO phonon fragments. This is consistent with the observed intensity changes in Fig. 3 and the loss of intensity in the TO mode associated with ILM formation in Refs. [5,6]. Next we note that for the NaI lattice without symmetry breaking there are two distinct atoms in the basis with 3 degrees of freedom each, resulting in six phonon branches: 2 TO branches, 2 TA branches, 1 LA branch, and 1 LO branch. Because of cubic symmetry the TO and TA branches are degenerate. Hence, the TO phonon share of the total density of states is $1/3$. Additionally, we assume that the ILM intensity is $1/3$ of the TO and that the fragments make up three equal parts of the remaining TO intensity. The $1/3$ estimate for the ILM peak intensity comes from an estimate made in Ref. [12] based on matching simulated intensities with the spectrum observed in Ref. [5] but should be considered a fairly rough estimate. The equal division of the TO phonon fragments follows from the zone-folding picture used to explain the fragmentation of the mode in Ref. [6]. Combining the appropriately weighted terms, the vibrational entropy difference in going from state II to state III in the high-temperature limit can be expressed in terms of mode frequencies as

$$\Delta S_{\text{vib}}^{\text{III-II}} = 3 k_B \left[\frac{1}{3} \ln \left(\frac{(\omega_{\text{ILM}}^{\text{II}})^{1/2} (\omega_{\text{TO}}^{\text{II}})^{2/3}}{(\omega_{\text{ILM}}^{\text{III}})^{1/3} (\omega_{\alpha}^{\text{III}})^{2/9} (\omega_{\beta}^{\text{III}})^{2/9} (\omega_{\gamma}^{\text{III}})^{2/9}} \right) + \frac{2}{3} (\text{remaining phonons}) \right]. \quad (2)$$

The frequencies of the modes are extracted directly from the spectral features in Fig. 2(a) and are indicated in the inset bubbles in Fig. 3. Plugging these frequencies into Eq. (2) and assuming a negligible contribution from the remaining phonons results in $\Delta S_{\text{vib}}^{\text{III-II}} = 0.026 k_B/\text{atom}$, which is in reasonable agreement with the total entropy change of $\Delta S_{\text{tot}}^{\text{III-II}} = 0.02 \pm 0.005 k_B/\text{atom}$ estimated from the heat capacity [Fig. 1(a)]. The same calculation for the transition from region III to region IV results in $\Delta S_{\text{vib}}^{\text{IV-III}} = 0.024 k_B/\text{atom}$, which is also in reasonable agreement with the total entropy change of $\Delta S_{\text{tot}}^{\text{IV-III}} = 0.02 \pm 0.005 k_B/\text{atom}$. Hence, the abrupt spectral changes associated with the breakup of the TO phonon observed in Fig. 2 can adequately explain the entropy changes indicated by the peaks in the heat capacity in Fig. 1(a) (see summary in Fig. 3).

B. Transition enthalpy from lattice distortions

The shifting of different order x-ray-diffraction reflections from the expected value, as found in Fig. 1(b), can be understood in terms of planar faults forming in the structure. Random planar faults that shift crystal planes by some amount with respect to other regions, when summed over many randomly placed faults, produce a phase shifting of the usual Bragg reflections [20]. This result was first derived by Hendricks and Teller [20] for layered structures, such as clays, but the formulation has since been extended to other systems, such as deformation faults in metals [19] and stacking faults in high-temperature superconductors [21]. In each of these cases, however, the faults are nonequilibrium defects in the crystal structure that can usually be guessed *a priori*, allowing a model to be constructed (e.g., random misplaced planes in a close-packed plane-stacking sequence [19]). Here, however, the structures are forming spontaneously in thermal equilibrium and are stabilized by the vibrational entropy of the dynamical structures that form with the planar faults. Furthermore, the shifts do not match those expected with conventional stacking faults in fcc materials. For example, conventional stacking faults on (111) planes in the fcc structure cause the (111) diffraction peak to shift to smaller effective d spacings, whereas the (200) diffraction peak shifts to larger effective d spacings [22]. Here, both (111) and (200) reflections shift to larger effective d spacings, see Fig. 1(b). For small layer distortions this result is not surprising since the peak shifts are only expected to oscillate rapidly with q for large local distortions. Very small distortions correspond to oscillations over a very broad range in q space, in which case it may only be possible to observe the initial rise in the peak shift. A more appropriate alternative limit is that of small layer distortion strains, which we derive below. However, to apply this approximation it is useful to first come up with a guess for a layered structure. In the case of going from state II to state III the dynamical superlattice structure described in Ref. [6] for state III, combined with the absence of any superlattice diffraction peaks in the synchrotron x-ray data measured here, provides a way to deduce a likely structure.

The absence of superlattice diffraction peaks, despite the presence of a dynamical superlattice of local modes [6], can be explained only if the localized mode polarization is somehow orthogonal to the ordering direction. This is because if the local modes were ordered in the same direction that they displace atoms, then small differences in the Debye-Waller factor associated with the local modes would be expected to give superlattice reflections even in the case of ILMs where the atom type is not different for the localized mode. Indeed, as described in Ref. [6] the ILMs in the dynamical superlattice are polarized along the [011] direction whereas ordering occurs along the [100] direction. Hence, a simple solution to the problem is that the ILM superlattices are ordered along [100]-type directions but in planes randomly stacked along the orthogonal [011]-type directions such that the ILMs are polarized out of the ordered plane as illustrated in Fig. 4(a). The random stacking of the planes with normal pointing along the ILM polarization direction explains the absence of superlattice reflections. This is because there are no mode displacements occurring in the ordering direction.

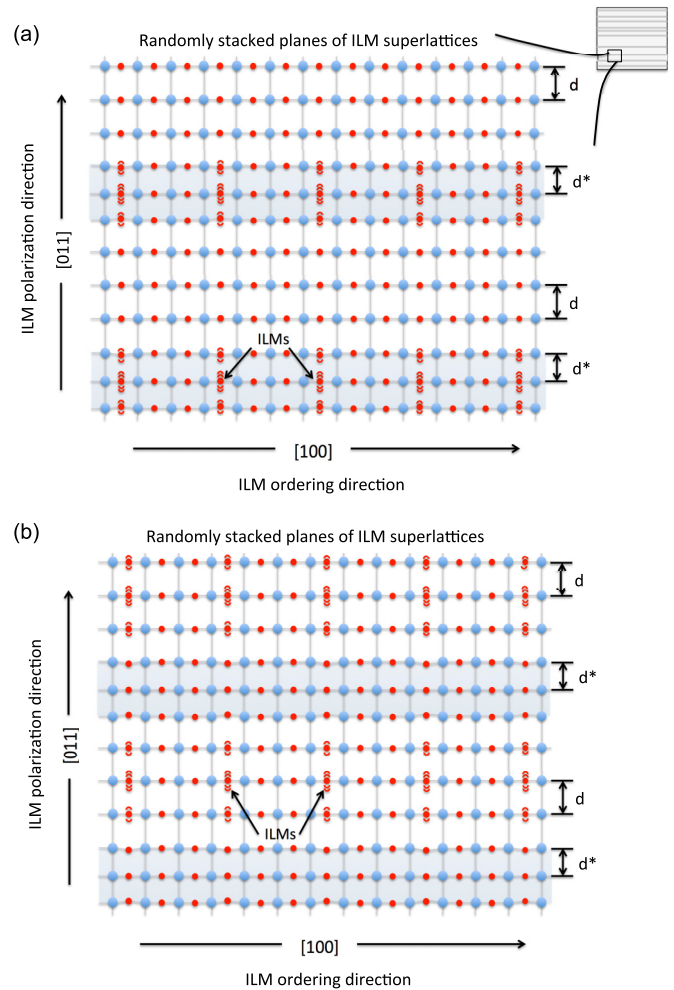


FIG. 4. (Color online) These illustrations show an arrangement of ILM superlattices [6] that might explain the observed dynamical and stacking-fault-like structures inferred from the measurements near 636 K. (a) The shaded areas indicate planes where the ILMs form a superlattice with the ILMs repeating every third site to explain the $q = 1/3$ scale in the dynamical superlattice, which is described in detail in Ref. [6] and partly summarized in Fig. 1(c). To explain the stacking-fault-like shifts in the diffraction peaks, it is assumed that these planes of dynamical superlattices (shaded areas) are stacked randomly along [011] while ordered along [100] and that the lattice spacing in the occupied planes d^* is different from the value of the unoccupied planes d . (b) A scenario similar to (a) except that the dynamical superlattice of the ILMs fills the larger regions between the faults.

Rather, the displacements, both static and dynamic, occur along the direction of random stacking, which would manifest as stacking-fault-like effects on the x-ray-diffraction peaks rather than superlattice reflections. The abrupt phase shifting of the (220) reflection at the transition into and out of the dynamical superlattice state near 636 K, Figs. 1 and 2, corroborates this picture and indicates that the lattice spacing at the plane occupied by the ILM superlattice d^* must differ from the value in the surrounding matrix d [20] [Fig. 4(a)].

The enthalpy of the transition from state II to state III (Fig. 1) can now be understood in terms of the strain energy of

forming the distorted planes illustrated in Fig. 4(a). Treating the scattering from (220) planes as a one-dimensional sum along the [220] direction [20], the shift in the (220) reflection diffraction angle $\Delta(2\theta)$ due to randomly stacked distorted planes can be written as [21]

$$\Delta(2\theta) = \frac{\lambda f}{2\pi d \cos \theta} \sin\left(2\pi \frac{d^*}{d}\right), \quad (3)$$

where $\lambda = 0.4133 \text{ \AA}$ (x-ray wavelength), $\theta = 0.0888 \text{ rad}$ [experimental diffraction angle for the (220) reflection], $\Delta(2\theta) = 0.0006 \text{ rad}$ [from an $\sim 0.3\%$ experimentally observed shift in the effective d spacing, Fig. 1(b)], $d = 2.33 \text{ \AA}$ (experimental), f is the occurrence frequency of the distorted planes, and d^* is the d spacing within the distorted planes (Fig. 4). Note that for small strains the ratio d^*/d is related to the strain at the distorted layer $\varepsilon = 1 - \frac{d^*}{d}$ and that $\sin(2\pi \frac{d^*}{d}) = \sin(2\pi \frac{d^*}{d} - 2\pi) = \sin[-2\pi(1 - \frac{d^*}{d})] = -\sin(2\pi\varepsilon) \cong -2\pi\varepsilon$. Hence, in the limit of small distortion strains the peak shift can be expressed as

$$\Delta(2\theta) \cong \left(\frac{-\lambda}{d \cos \theta}\right) f \varepsilon \quad (4\varepsilon \ll 1). \quad (4)$$

From this expression it can be seen that for small layer strains the peak shift simply becomes proportional to the product of the layer strain and the layer frequency. Substituting in the values of the known quantities into Eq. (4) we obtain $f\varepsilon = -0.003$. This distributed strain can now be used to evaluate the strain-energy cost of forming the elastic distortions, which we equate to the transition enthalpy.

A solution where the distortion strain energy is consistent with the observed transition enthalpy can be found by setting $f = 1/10$, which corresponds to a strain in each distorted layer of -3% (contraction). In other words, the $\sim 0.3\%$ apparent contraction in the d spacing for the (220) reflection [Fig. 1(b)] corresponds to a 3% contraction occurring randomly for 1/10 of the planes. For a uniform elastic strain, the strain-energy density is given by $u = \frac{1}{2}E\varepsilon^2$, where E is Young's modulus (for NaI $E \cong 9.7 \text{ GPa}$ and the molar density is 24.28 kmol/m^3). From this equation it can be shown that a uniform elastic strain of 3% gives a strain-energy density of 178 J/mol . Since we are assuming the strained layers make up 1/10 of the layers, an average energy density contributed by a particular (110)-type set of planes is 17.8 J/mol . There are, however, six equivalent (110)-type planes and assuming all (110)-type planes behave the same way the total energy density is 107 J/mol . This energy is consistent with the transition enthalpy $\Delta H_{\text{tot}}^{\text{III-II}}$ expected from the heat capacity (Fig. 3) since $\Delta H_{\text{tot}}^{\text{III-II}} = T_t \Delta S_{\text{tot}}^{\text{III-II}} = (622 \text{ K})(0.02 k_B/\text{atom}) = 104 \text{ J/mol}$, where T_t is the transition temperature (more precisely, $f = 10.3\%$ gives 104 J/mol). Larger values for f decrease this calculated strain energy, and smaller values increase the calculated strain energy. The value of $f = 1/10$ provides a consistent solution for the observed peak shift and transition enthalpy.

A distorted fault layer frequency $f = 1/10$ is high enough to introduce ambiguity regarding the location of the dynamical superlattice structures since they could equally well be located in the narrow fault, Fig. 4(a), or within the larger regions between the narrow faults, Fig. 4(b). In

either case the coherence length would be sufficiently short to explain the absence of superlattice reflections. However, the pronounced effects on the lattice dynamics (Fig. 2) indicate that dynamical superlattice structures, which fully split the TO phonon [Fig. 2(a)], are extensive and, therefore, tend to favor the dynamical superlattices existing within the larger regions between the faults, Fig. 4(b). In other words, if the dynamical superlattices were forming within only $\sim 10\%$ of the regions [Fig. 4(a)] the TO phonon would not be fully split, and the expected spectra would be a superposition of split and unsplit TO phonons, rather than the complete splitting observed [Fig. 2(a)].

Although the dynamical superlattice effect [6] only occurs in a narrow temperature range, the distortion-fault shifts in the x-ray-diffraction reflections appear to occur at all of the temperatures where the localized modes are observed [5,6], Fig. 1. This suggests that the observed localization occurs within planes at all temperatures, but that dynamical superlattice formation only occurs in these planes at some temperatures (e.g., Ref. [6]). The absence of dilations in the bulk volume [Fig. 1(a)] also indicates that the internal distortions tend to conserve volume, meaning that the contractions in some layers are made up for by expansions in other layers. This is not that surprising for distortions driven by the anharmonic localization of lattice vibrations. Extended anharmonic lattice vibrations contribute a uniform thermal expansion to the crystal, and thus the localization or redistribution of the lattice vibrations is expected to localize or redistribute thermal expansion rather than simply add to it [23].

V. DISCUSSION

The coincidence of stacking-fault-type diffraction peak shifts developing at the same temperatures where ILMs [5] and dynamical superlattices [6] are observed (Figs. 1 and 2), provides strong evidence that these dynamical features are, in fact, forming within randomly stacked two-dimensional structures, rather than as isolated point-defect-like ILMs [5]. This argument is made more convincing by the fact that the observed reflection-order-dependent diffraction peak shifts are not expected with point- or line-defect-type breaks in the symmetry [19], meaning they must come from planar distortions in the structure [20]. The spontaneous changes in the dynamical structures and planar distortions with commensurate heat-capacity peaks, vibrational entropy, and internal strain-energy changes, indicate that these dynamical structures are part of the equilibrium thermodynamics of NaI but are not stabilized by configurational entropy. The equilibrium thermodynamics are therefore distinct from that of the vacancy or point-defect formation mechanism where configurational entropy is assumed to stabilize an equilibrium concentration of point defects or possibly ILMs [4]. The two-dimensional structures are also clearly distinct from conventional stacking faults since conventional stacking faults do not form spontaneously in thermal equilibrium, and they do not exhibit consecutive transitions between structures differing only slightly in internal strain energy and vibrational entropy. The key role of vibrational entropy, in particular, shows that the formation of the faulting structures must be driven by the dynamical structures as opposed to merely being the

dynamical consequences of structural faults formed by some other mechanism.

The observed transitions are also unlike soft-phonon-driven phase transitions, such as with ferroelectric [1] or shape-memory martensitic transitions [24]. With these transitions, the crystal symmetry is lowered on cooling to obtain a lower electronic-energy ground state, such as with a Peierls distortion, whereas here the symmetry is lowered (at least partially) on heating as the lower-symmetry dynamical structures are stabilized by increases in vibrational entropy.

These dynamical structures are reminiscent of the dynamical patterns that occur in driven anharmonic lattices in both two dimensions [25,26] and in one dimension [27]. Solitons and pattern formation are also common in nonlinear systems driven far from equilibrium [28,29], and early demonstrations of soliton patterns date back to the classic paper of Korteweg and de Vries in 1895 [30]. More recently, molecular dynamics simulations of superheated metallic Ni crystals suggest that stringlike cooperative motion acts as a nonlinear dynamical mechanism in homogeneous melting [31]. In this context, it is interesting to note that the planar dynamical structures discovered here continue evolving with temperature and probably do so right up until NaI melts at 934 K. It is possible that these dynamical structures play an active role in the melting of NaI. Future work will explore this possibility and the possibility that similar dynamical structures and distortion faulting occur in related materials at high temperatures.

VI. CONCLUSIONS

Our results demonstrate that the localization observed in the lattice dynamics of NaI and interpreted as three-dimensional pointlike ILMs [5] is actually occurring along one dimension in randomly stacked planes. The random stacking combined with the cubic symmetry averaging gives the impression that localization is three dimensional, but the faulting effect in x-ray-diffraction peak shifts reported here clearly shows that the localization is occurring in random planes. This finding also explains why the dynamical ordering observed in the lattice dynamics is not detected in the average crystal structure [6]. These planar dynamical structures have different energetics

than that proposed for the pointlike ILMs. Rather than being stabilized by the configurational entropy of disordered pointlike ILMs, it is the vibrational entropy of the planar dynamical structures that stabilizes the formation of surrounding elastic distortions. Many variants of these dynamical structures, each with only small free-energy differences from the others, leads to a near continuous series of transitions with increasing temperatures, probably all the way up to melting. These transitions represent a new class of phase transitions that are defined more by symmetry breaking in the lattice-dynamical structure than in the average crystal, electronic, or magnetic structure.

ACKNOWLEDGMENTS

We would like to thank W. J. Evans, D. Ruddle, and K. Visbeck for assistance with the high-temperature furnace used in these experiments. We would also like to thank N. Agladze for assistance with and discussions on the dilatometry and differential scanning calorimetry measurements. Research sponsored, in part (M.E.M.), by the U.S. Department of Energy, Office of Basic Energy Sciences, Materials Sciences and Engineering Division. Portions of this work (J.R.J. and N.P.B.) were supported by LDRD (Tracking Code No. 14-ERD-041) at Lawrence Livermore National Laboratory (LLNL). LLNL is operated by Lawrence Livermore National Security, LLC, for the U.S. Department of Energy, National Nuclear Security Administration under Contract No. DE-AC52-07NA27344. Portions of this work were performed at HPCAT (Sector 16), Advanced Photon Source (APS), Argonne National Laboratory. HPCAT is supported by CIW, CDAC, UNLV, and LLNL through funding from the DOE-NNSA, DOE-BES, and NSF. Beam time was graciously provided through CDAC. Use of the Advanced Photon Source, an Office of Science User Facility operated for the U.S. DOE Office of Science by Argonne National Laboratory, was supported by the U.S. DOE under Contract No. DE-AC02-06CH11357. The portion of this research performed at the Oak Ridge National Laboratory's Spallation Neutron Source was sponsored by the U.S. Department of Energy, Office of Basic Energy Sciences.

-
- [1] J.-C. Toledano and P. Toledano, *The Landau Theory of Phase Transitions: Application to Structural, Incommensurate, Magnetic and Liquid Crystal Systems*, World Scientific Lecture Notes in Physics (World Scientific, Singapore, 1987), Vol. 3.
 - [2] E. W. Montroll, G. H. Weiss, and A. A. Maradudin, *Theory of Lattice Dynamics in the Harmonic Approximation*, Solid State Physics, Sup. 3 (Academic, New York, 1968).
 - [3] S. Flach and A. V. Gorbach, *Phys. Rep.* **467**, 1 (2008).
 - [4] A. J. Sievers and S. Takeno, *Phys. Rev. Lett.* **61**, 970 (1988).
 - [5] M. E. Manley, A. J. Sievers, J. W. Lynn, S. A. Kiselev, N. I. Agladze, Y. Chen, A. Llobet, and A. Alatas, *Phys. Rev. B* **79**, 134304 (2009).
 - [6] M. E. Manley, D. L. Abernathy, N. I. Agladze, and A. J. Sievers, *Sci. Rep.* **1**, 4 (2011).
 - [7] F. Wilczek, *Phys. Rev. Lett.* **109**, 160401 (2012).
 - [8] A. Shapere and F. Wilczek, *Phys. Rev. Lett.* **109**, 160402 (2012).
 - [9] T. Li, Z.-X. Gong, Z.-Q. Yin, H. T. Quan, X. Yin, P. Zhang, L.-M. Duan, and X. Zhang, *Phys. Rev. Lett.* **109**, 163001 (2012).
 - [10] L. Z. Khadeeva and S. V. Dmitriev, *Phys. Rev. B* **84**, 144304 (2011).
 - [11] A. A. Kistanov and S. V. Dmitriev, *Phys. Solid State* **54**, 1648 (2012).
 - [12] A. J. Sievers, M. Sato, J. B. Page, and T. Rössler, *Phys. Rev. B* **88**, 104305 (2013).
 - [13] L. D. Landau and E. M. Lifshitz, *Statistical Physics*, 3rd ed., Part 1 (Pergamon, Oxford, 1980), p. 85.
 - [14] M. Kempa, P. Ondrejko, P. Bourges, P. Marton, and J. Hlinka, *Phys. Rev. B* **89**, 054308 (2014).

- [15] A. D. B. Woods, W. Cochran, and B. N. Brockhouse, *Phys. Rev.* **119**, 980 (1960).
- [16] R. T. Azuah, L. R. Kneller, Y. Qiu, P. L. W. Tregenna-Piggott, C. M. Brown, J. R. D. Copley, and R. M. Dimeo, *J. Res. Natl. Inst. Stand. Technol.* **114**, 341 (2009).
- [17] J. A. Cape and G. W. Lehman, *J. Appl. Phys.* **34**, 1909 (1963).
- [18] G. W. H. Höhne, *Thermochim. Acta* **22**, 347 (1978).
- [19] B. E. Warren, *X-ray Diffraction* (Dover, New York, 1968), p. 288.
- [20] S. Hendricks and E. Teller, *J. Chem. Phys.* **10**, 147 (1942).
- [21] S. H. Wee, E. D. Specht, C. Cantoni, Y. L. Zuev, V. Maroni, W. Wong-Ng, G. Liu, T. J. Haugan, and A. Goyal, *Phys. Rev. B* **83**, 224520 (2011).
- [22] B. Fultz and J. M. Howe, *Transmission Electron Microscopy and Diffraction of Materials* (Springer-Verlag, Berlin, 2001), p. 447.
- [23] M. E. Manley, *Acta Mater.* **58**, 2926 (2010).
- [24] J. C. Lashley, S. M. Shapiro, B. L. Winn, C. P. Opeil, M. E. Manley, A. Alatas, W. Ratcliff, T. Park, R. A. Fisher, B. Mihaila, P. Riseborough, E. K. H. Salje, and J. L. Smith, *Phys. Rev. Lett.* **101**, 135703 (2008).
- [25] V. M. Burlakov, *Phys. Rev. Lett.* **80**, 3988 (1998).
- [26] V. M. Burlakov, *Int. J. Mod. Phys. B* **13**, 791 (1999).
- [27] R. Khomeriki, S. Lepri, and S. Ruffo, *Phys. Rev. E* **64**, 056606 (2001).
- [28] O. A. Dubovsky and A. V. Orlov, *Phys. Solid State* **52**, 899 (2010).
- [29] M. C. Cross and P. C. Hohenberg, *Rev. Mod. Phys.* **65**, 851 (1993).
- [30] D. J. Korteweg and G. de Vries, *Philos. Mag.* **39**, 422 (1895).
- [31] H. Zhang, M. Khalkhali, Q. Liu, and J. F. Douglas, *J. Chem. Phys.* **138**, 12A538 (2013).